Research Article

Controlled Ag-driven superior rate-capability of Li₄Ti₅O₁₂ anodes for lithium rechargeable batteries

Jae-Geun Kim[1], Dongqi Shi[1], Min-Sik Park[2], Goojin Jeong[2] (✉), Yoon-Uk Heo[3], Minsu Seo[2], Young-Jun Kim[2], Jung Ho Kim[1] (✉), and Shi Xue Dou[1]

[1] Institute for Superconducting and Electronic Materials, University of Wollongong, North Wollongong, NSW 2500, Australia

[2] Advanced Batteries Research Center, Korea Electronics Technology Institute, Seongnam 463-816, Republic of Korea

[3] Research Facility Center, Graduate Institute of Ferrous Technology, Pohang University of Science and Technology, Pohang 790-784, Republic of Korea

ABSTRACT

The morphology and electronic structure of a $Li_4Ti_5O_{12}$ anode are known to determine its electrical and electrochemical properties in lithium rechargeable batteries. $Ag–Li_4Ti_5O_{12}$ nanofibers have been rationally designed and synthesized by an electrospinning technique to meet the requirements of one-dimensional (1D) morphology and superior electrical conductivity. Herein, we have found that the 1D $Ag–Li_4Ti_5O_{12}$ nanofibers show enhanced specific capacity, rate capability, and cycling stability compared to bare $Li_4Ti_5O_{12}$ nanofibers, due to the Ag nanoparticles (<5 nm), which are mainly distributed at interfaces between $Li_4Ti_5O_{12}$ primary particles. This structural morphology gives rise to 20% higher rate capability than bare $Li_4Ti_5O_{12}$ nanofibers by facilitating the charge transfer kinetics. Our findings provide an effective way to improve the electrochemical performance of $Li_4Ti_5O_{12}$ anodes for lithium rechargeable batteries.

1 Introduction

Ti-based oxide anode materials have attracted much attention due to their potential advantages, which include excellent thermal stability, low cost, and environmental friendliness [1, 2]. In particular, spinel $Li_4Ti_5O_{12}$ has been intensively studied as a promising anode to meet the requirements for electric vehicles (EVs) and large-scale energy storage systems (ESSs)

[3–6]. It is well known that $Li_4Ti_5O_{12}$ shows some promise, largely due to its two key advantages: (i) long cycle life arising from its zero-strain structure and (ii) little electrolyte decomposition due to its higher equilibrium potential, showing a voltage plateau at 1.55 V vs. Li/Li^+ [7–9]. In addition, $Li_4Ti_5O_{12}$ can store three Li^+ ions per formula unit (rock-salt phase), with a theoretical capacity of 175 mA·h·g⁻¹ [10]. $Li_4Ti_5O_{12}$ has a low electrical conductivity of about 10^{-13} S·cm⁻¹ [11],

however, resulting in poor rate capability and an initial capacity loss. To improve this, several methods have been considered to enhance the electrical conductivity. The most efficient methods involve applying a surface coating or doping to achieve metallic substitution [12–23]. Surface coating with a conductive material, such as carbon, is not an ideal solution, because it is hard to make a homogeneous thin layer. Severe aggregation of metallic additives is also known to be difficult to avoid.

According to our previous work [24], one-dimensional (1D) nanostructures have remarkable electrical, thermal, and mechanical properties. It is accepted that 1D nanostructures have clear morphological advantages due to the shortened Li^+ diffusion pathways and improved electron transport in lithium rechargeable batteries. Compared to other complicated synthetic methods, the electrospinning method suggested in this study can readily fabricate 1D nanostructures with various diameters, compositions, and morphologies, including hollow structures and uniaxially aligned arrays [25–33]. Furthermore, it enables mass production for commercialization with multiple nozzles and is capable of any sort of metallic doping. Even although the synthesis of small-sized $Li_4Ti_5O_{12}$ particles through solid-state reaction, hydrothermal, or sol–gel methods is known to be the most direct approach [34–36], using these methods with metallic dopants/additives usually leads to severe inhomogeneity or difficulty in mass production [37]. Liu et al. reported that Ag nanoparticles (<10 nm in size) located within $Li_4Ti_5O_{12}$ particles led to improved rate performance and long cycling life due to enhanced electrical conductivity [38]. However, no quantitative analysis has ever been carried out. From this point of view, it might be expected that the electrochemical performance of 1D $Li_4Ti_5O_{12}$ nanostructures in energy storage could be improved if metal nanoparticles were distributed all throughout the $Li_4Ti_5O_{12}$ material. To the best of our knowledge, a 1D architecture of $Li_4Ti_5O_{12}$ with incorporation of Ag nanoparticles has never been reported, and we expect that the Ag additive might improve the electrochemical performance of $Li_4Ti_5O_{12}$ nanofibers by enhancing intra- or inter-grain connectivity. In this context, we report a simple one-step synthesis for 1D Ag–$Li_4Ti_5O_{12}$ nanofibers using the electrospinning method. The as-

prepared Ag–$Li_4Ti_5O_{12}$ nanofibers show excellent rate capability and cycling stability with enhanced electrical conductivity and maximized kinetic properties because of the shortened diffusion length for Li^+ transport and the fast electron transport.

2 Experimental

2.1 Bare $Li_4Ti_5O_{12}$ and Ag–$Li_4Ti_5O_{12}$ nanofibers and their structural characterization

For the $Li_4Ti_5O_{12}$ nanofibers, 1.48 mL of titanium(Ⅳ) isopropoxide and 0.413 g of lithium acetate were mixed with 10 mL of ethanol and 7 mL of acetic acid. After dissolving over 1 h, 0.8 g of polyvinylpyrrolidone (PVP) was added to this solution, followed by magnetic stirring for 1 h. For Ag-doped $Li_4Ti_5O_{12}$ nanofibers, 0.045 g of silver nitrate was dissolved in 16 mL of ethanol and 1.48 of mL of titanium(Ⅳ) isopropoxide, and 0.413 g of lithium acetate and 1 mL of acetic acid were added to the dissolved Ag salt solution. The yellow transparent solution was immediately loaded into a plastic syringe equipped with a 23 gauge needle. The needle was connected to a high voltage supply, and the feed rate for the precursor was set at 0.7 mL·h^{-1}. A distance of 13 cm and a voltage of 20 kV were maintained between the tip of the needle and a drum collector. A schematic illustration of the electrospinning set-up for obtaining $Li_4Ti_5O_{12}$ and Ag–$Li_4Ti_5O_{12}$ nanofibers is shown in Fig. 1(a). After the electrospinning, the electrospun nanofibers were detached from the drum collector. Finally, the nanofibers were heat-treated at 750 °C for 3 h in air. The morphology and microstructure of the nanofibers were characterized by X-ray diffraction (XRD), field emission-scanning electron microscopy (FE-SEM), and transmission electron microscopy (TEM).

2.2 Electrochemical performance

The electrodes were prepared by coating aluminum foil substrates with slurries containing the active material, carbon black (Super-P), and polyvinylidene fluoride (PVDF) in a weight ratio of 80:10:10 using N-methylpyrrolidone (NMP) as the solvent. After coating the slurry on Al foil, the electrodes were dried at 120 °C for 12 h under vacuum. The mass of the active
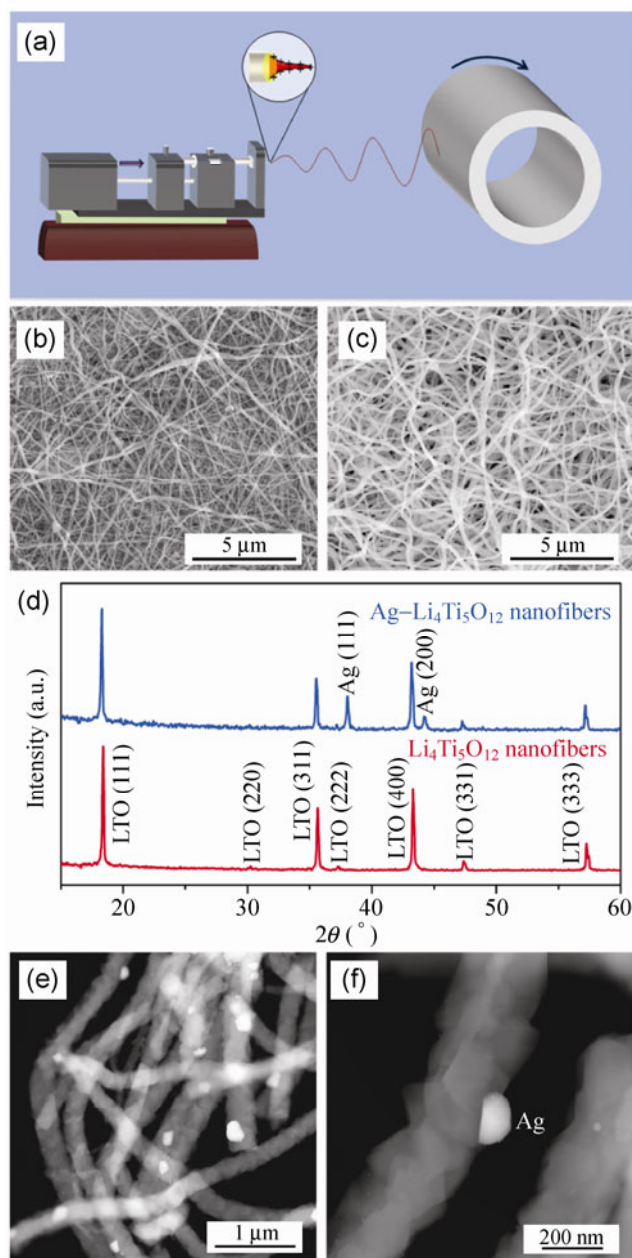
Figure 1 (a) Schematic illustration of the electrospinning apparatus. SEM images of (b) $Li_4Ti_5O_{12}$ and (c) $Ag–Li_4Ti_5O_{12}$ nanofibers after calcination. (d) XRD patterns of $Li_4Ti_5O_{12}$ and $Ag–Li_4Ti_5O_{12}$ nanofibers after calcination at 750 °C. (e) and (f) HAADF STEM images of $Ag–Li_4Ti_5O_{12}$ nanofibers

material was approximately 2 mg·cm^{-2}. 2,032 coin cells were assembled in a dry room. A porous polyethylene film was used as the separator, 1 M $LiPF_6$ dissolved in a 1:2 (by volume) mixture of ethylene carbonate (EC) and dimethyl carbonate (DMC) was employed as the electrolyte solution, and lithium foil was used as the counter electrode. Discharge (Li$^+$ intercalation)–charge

(Li$^+$ de-intercalation) tests were performed for up to 200 cycles in a voltage window of 1 to 3 V (vs. Li/Li$^+$). The first and second cycles were conducted galvanostatically at a current density of 0.1 C (where 1 C was set as 170 mA·g^{-1}), and measurements of the rate capability at various current densities and cycling tests at 1 C were performed. Electrochemical impedance spectroscopy (EIS) was performed after the first discharge with a three-electrode electrochemical system, in which the reference and counter electrodes were Li metal. The EIS frequency ranged from 10^6 to 10^{-2} Hz, and the voltage perturbation amplitude was 5 mV. Data acquisition and analysis were carried out using the electrochemical impedance software packages ZPlot and ZView (Version 3.0, Scribner Associates, Inc., USA), respectively.

3　Results and discussion

The morphology and crystalline microstructure of the two kinds of nanofibers were directly confirmed by XRD, SEM, and TEM analyses. As shown in Figs. 1(b) and 1(c), only small differences were observed between the bare $Li_4Ti_5O_{12}$ (LTO) and the $Ag–Li_4Ti_5O_{12}$ nanofibers. The randomly aligned nanofibers have average diameters of 50–200 nm and lengths extending to several tens of micrometers. Interestingly, it is hard to distinguish the Ag particles in the SEM image of $Ag–Li_4Ti_5O_{12}$ nanofibers in Fig. 1(c). From the XRD patterns in Fig. 1(d), however, we found that all reflections were identical to the standard peaks of $Li_4Ti_5O_{12}$ and metallic Ag. This indicates that the $Li_4Ti_5O_{12}$ and $Ag–Li_4Ti_5O_{12}$ nanofibers were successfully synthesized during the heat treatment without introducing any impurity such as rutile TiO_2. The microstructure of the $Ag–Li_4Ti_5O_{12}$ nanofibers was further observed by high-angle annular dark-field (HAADF) scanning TEM (STEM), as shown in Figs. 1(e) and 1(f). The $Ag–Li_4Ti_5O_{12}$ nanofibers exhibited smooth and uniform surfaces, and the Ag particles were distinguished in the STEM images by their bright contrast. We were able to conclusively prove that the $Ag–Li_4Ti_5O_{12}$ nanofibers have the form of a secondary 1D $Ag–Li_4Ti_5O_{12}$ composite consisting of Ag and $Li_4Ti_5O_{12}$ primary particles, as shown in Fig. 1(f).

The schematic diagram of the structure of an

Ag–Li$_4$Ti$_5$O$_{12}$ nanofiber in Fig. 2(a) illustrates the TEM results. The Ag particles (~100 nm) have been successfully incorporated and are interconnected between the Li$_4$Ti$_5$O$_{12}$ nanoparticles, as can be seen in Fig. 2(b). These interconnected Ag particles improve the electrical contact between the Li$_4$Ti$_5$O$_{12}$ particles and the current collector. Furthermore, the Ag nanoparticles were observed to be less than 5 nm in size, mostly spherical in shape, and embedded in the Li$_4$Ti$_5$O$_{12}$ host matrix (Fig. 2(c)). In fine detail, the high-resolution TEM (HRTEM) images confirmed that the interconnected Ag particles were single-crystal from their selected area electron diffraction (SAED) patterns, and the exposed surfaces of the Ag particles were determined
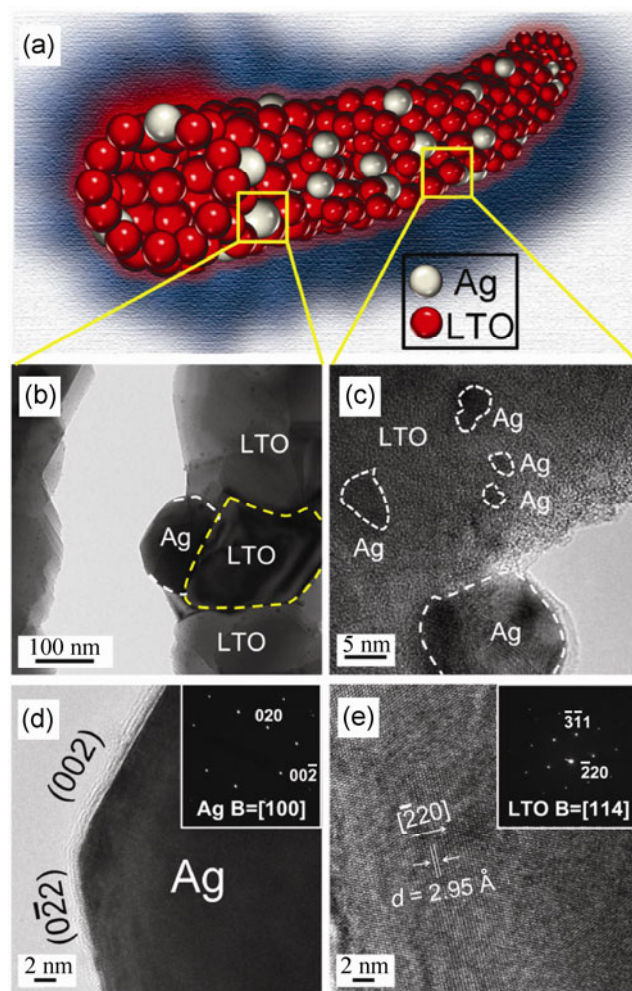

Figure 2 (a) Schematic illustration of Ag–Li$_4$Ti$_5$O$_{12}$ nanofibers. (b) and (c) Low magnification TEM images of Ag–Li$_4$Ti$_5$O$_{12}$ nanofibers. HRTEM images of (d) Ag and (e) Li$_4$Ti$_5$O$_{12}$ nanoparticles and the corresponding SAED patterns.

to be {002} and {0$\bar{2}$2} facets, as shown in Fig. 2(d). The Li$_4$Ti$_5$O$_{12}$ particles also show a highly crystalline structure. The lattice spacing parallel to the side wall is ~2.95 Å, in accordance with the ($\bar{2}$20) planes of Li$_4$Ti$_5$O$_{12}$ as shown in Fig. 2(e). As a result, the two important configurations that could enhance the electrical conductivity are (i) interconnected large-sized Ag particles and (ii) embedded Ag nanoparticles. It is generally argued that embedded Ag nanoparticles mainly play a supporting role in term of electrical conductivity, and it is difficult to conclude that they are the predominant factor. For that purpose, the interface between the Li$_4$Ti$_5$O$_{12}$ particles was further investigated using a Cs-corrected STEM, as shown in Fig. 3. Here, the nanosized Ag particles were observed to be concentrated along the grain boundaries. Their size was less than 5 nm, which can improve charge transfer between the Li$_4$Ti$_5$O$_{12}$ nanoparticles, predominantly due to enhanced electrical conductivity. The insets show the grain boundaries (dashed lines) and Ag nanoparticles (dots). If conducting agents, such as RuO$_2$ or Fe$_2$P, were distributed at the boundaries of active material, it would affect rate capability due to the enhanced electrical conductivity, according to the literature [23, 39]. In our study, Li$_4$Ti$_5$O$_{12}$ primary particles have an intimate electrical contact with the aid of Ag particles at the grain boundaries, and this might be effective for fast electron transfer. We thus argue that since the Ag particles could be observed all over the Li$_4$Ti$_5$O$_{12}$ nanofibers, this would be expected to enhance electrochemical performance.

To explore the possibility of using Ag–Li$_4$Ti$_5$O$_{12}$ nanofibers as the anode in Li rechargeable batteries, galvanostatic discharge–charge cycling was carried out to investigate the lithium storage properties of the Li$_4$Ti$_5$O$_{12}$ and Ag–Li$_4$Ti$_5$O$_{12}$ nanofibers. Figure 4(a) shows the first discharge–charge voltage profiles of the Li$_4$Ti$_5$O$_{12}$ and Ag–Li$_4$Ti$_5$O$_{12}$ nanofibers at a current density of 0.1 C. The discharge and charge capacities of the Ag–Li$_4$Ti$_5$O$_{12}$ nanofibers were 195.7 and 164.2 mA·h·g^{-1}, respectively, in the first cycle. They exhibited a larger initial discharge capacity than the bare Li$_4$Ti$_5$O$_{12}$ nanofibers (178.1 mA·h·g^{-1}). The initial irreversible capacities of both types of nanofibers were estimated to be 21.1 (Li$_4$Ti$_5$O$_{12}$) and 31.5 mA·h·g^{-1} (Ag–Li$_4$Ti$_5$O$_{12}$).
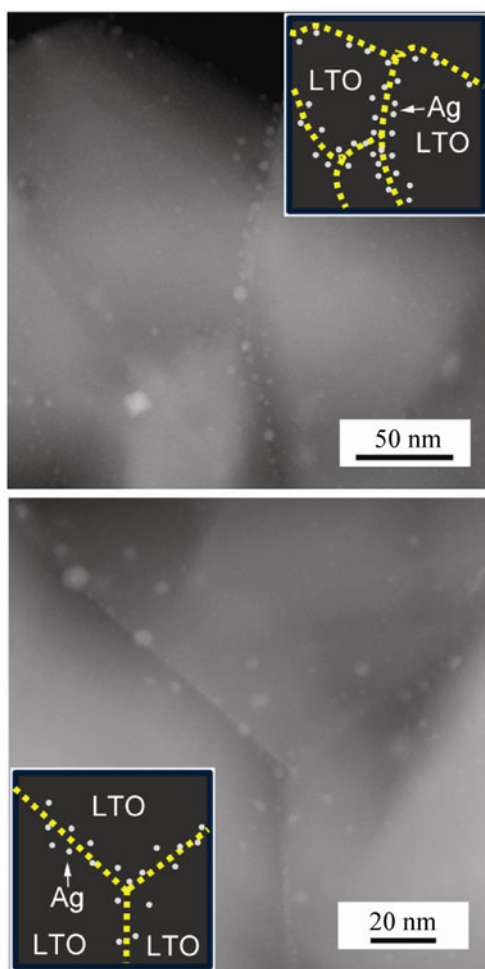
Figure 3 HAADF STEM images of grain boundaries in Ag–$Li_4Ti_5O_{12}$ nanofibers. The insets show the grain boundaries (dashed lines) and Ag particles (dots).

Although the Ag–$Li_4Ti_5O_{12}$ exhibited a slightly larger initial irreversible capacity, which probably originated from different electrolyte decomposition behavior [21, 41], this electrode still showed increased reversible capacity compared to the bare $Li_4Ti_5O_{12}$. The rate-capability and cycling performances of the $Li_4Ti_5O_{12}$ and Ag–$Li_4Ti_5O_{12}$ nanofibers were also evaluated at various current rates from 0.1 to 30 C, as shown in Fig. 4(b). The Ag–$Li_4Ti_5O_{12}$ nanofibers show enhanced rate performance compared to the bare $Li_4Ti_5O_{12}$ nanofibers at all current rates. At current densities below 10 C, the capacities of the Ag–$Li_4Ti_5O_{12}$ nanofibers vary from 150 to 165 $mA·h·g^{-1}$. Furthermore, the Ag–$Li_4Ti_5O_{12}$ nanofibers still have a specific capacity of 140 $mA·h·g^{-1}$ at the high current density of 10 C, which is larger than that of the bare $Li_4Ti_5O_{12}$ nanofibers.
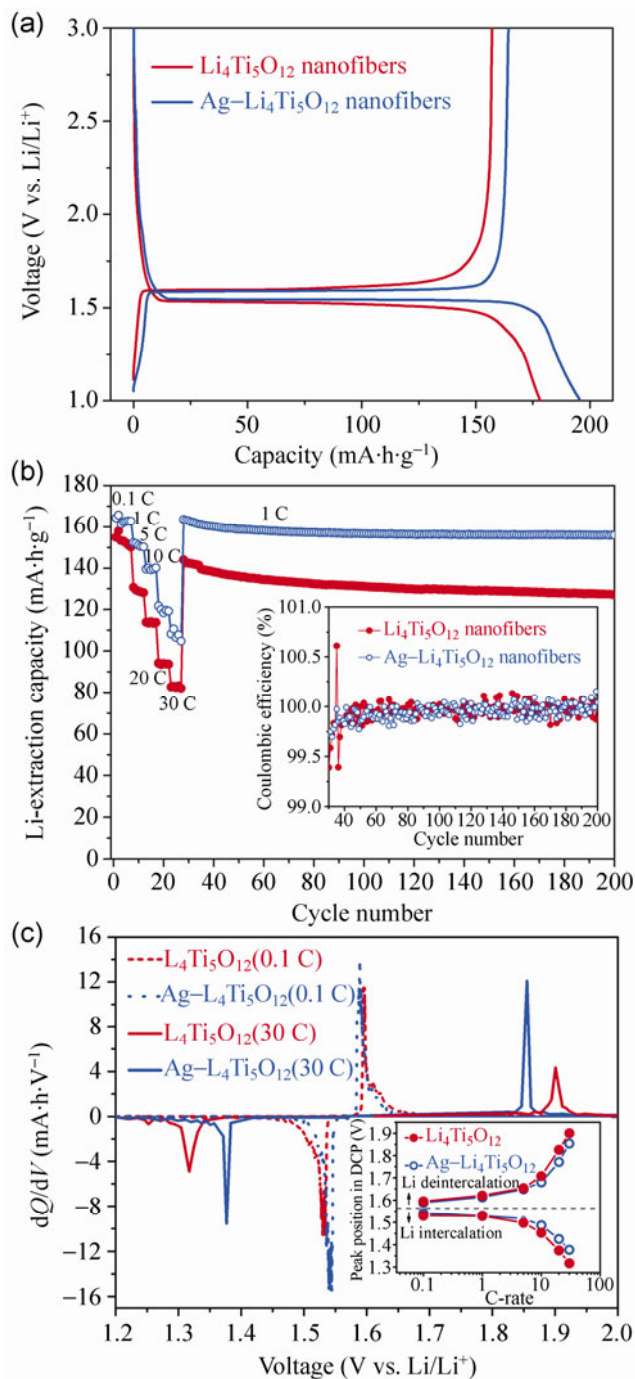

Figure 4 (a) Discharge–charge curves in the first cycle, (b) rate performance and coulombic efficiency (inset), and (c) differential capacity (dQ/dV) vs. voltage curves of $Li_4Ti_5O_{12}$ and Ag–$Li_4Ti_5O_{12}$ nanofibers, with the inset showing the overpotentials of the samples at different current densities.

Most notably, the Ag–$Li_4Ti_5O_{12}$ nanofibers exhibit remarkable rate performance at 10 C, which is much better than the performances of carbon-coated, surface-nitrided, phosphidated, or nanostructured $Li_4Ti_5O_{12}$

materials reported in the literature [14, 28, 41, 42]. At the highest rate of 30 C, corresponding to a time of 2 min to fully discharge/charge the materials, the specific capacity of the Ag–$Li_4Ti_5O_{12}$ nanofibers is 107.5 mA·h·g^{-1}, which is significantly higher than that of the bare $Li_4Ti_5O_{12}$ nanofibers (82.2 mA·h·g^{-1}). After the galvanostatic rate capability test, an additional cycling performance test was carried out at a current density of 1 C. The Ag–$Li_4Ti_5O_{12}$ nanofibers regained their Li$^+$ de-intercalation capacity of around 163.5 mA·h·g^{-1}, while further cycling led to a capacity of around 160 mA·h·g^{-1} being retained after 200 cycles. Figure 4(c) shows differential capacity plots of the $Li_4Ti_5O_{12}$ and Ag–$Li_4Ti_5O_{12}$ nanofibers at various current densities. The inset figure shows the overpotential of both nanofibers at various current densities from 0.1 to 30 C. Even if there is only a small difference in overpotential between the bare $Li_4Ti_5O_{12}$ nano-fibers and the Ag–$Li_4Ti_5O_{12}$ nanofibers at 0.1 C, the Ag–$Li_4Ti_5O_{12}$ nanofibers exhibit significantly lower overpotential than the bare $Li_4Ti_5O_{12}$ nanofibers with increasing current density, which results from a decrease in the polarization resistance because of the improved electrical conductivity of the Ag–$Li_4Ti_5O_{12}$ nanofibers. These results indicate that the superior rate capability and cycling performance can be attributed to the increased electrical conductivity of the $Li_4Ti_5O_{12}$ nanofibers due to the incorporation of Ag nanoparticles, which greatly enhances the charge transport during the charge/discharge process and thus leads to significant improvement in the electrochemical performance.

EIS measurements were also conducted to examine the internal conductivity of the $Li_4Ti_5O_{12}$ and Ag–$Li_4Ti_5O_{12}$ nanofibers. Nyquist plots of the AC-impedance spectra obtained for the lithiated $Li_4Ti_5O_{12}$ and Ag–$Li_4Ti_5O_{12}$ nanofibers are presented in Fig. 5. The parameters were determined by the complex nonlinear least squares (CNLS) fitting method with an equivalent circuit (inset) and are summarized in Table 1. R_{el} is the resistance of the electrolyte solution, the high frequency semicircle can be attributed to the surface layer resistance associated with the solid electrolyte interphase (R_{SEI}), and the medium frequency semicircle indicates the charge transfer resistance (R_{ct}) at the interface between the electrolyte and the electrode
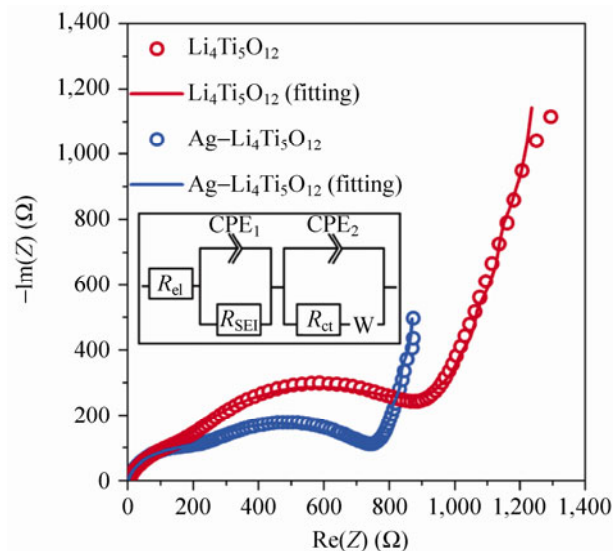

Figure 5 Nyquist plots of the $Li_4Ti_5O_{12}$ and Ag–$Li_4Ti_5O_{12}$ nanofibers. The inset figure shows the equivalent circuit used to interpret the impedance spectra.

Table 1 Best-fit values of EIS data with the equivalent circuit in Fig. 5.

	L$_4$Ti$_5$O$_{12}$ (Ω)	Ag–L$_4$Ti$_5$O$_{12}$ (Ω)
R_{SEI}	263	203
R_{ct}	1143	788

material. The more modest medium frequency semicircle of the Ag–$Li_4Ti_5O_{12}$ nanofibers (788 Ω) compared to that of the $Li_4Ti_5O_{12}$ nanofibers (1,143 Ω) clearly proves that the electrode material with incor-porated Ag particles features enhanced charge transfer due to improved electrical conductivity. The inclined lines in the Warburg region correspond to the Li$^+$ diffusion process inside the electrode material (W). The Ag–$Li_4Ti_5O_{12}$ nanofibers exhibit a larger slope than the bare $Li_4Ti_5O_{12}$ nanofibers, which implies high Li$^+$ mobility in the solid phase [43]. This result clearly demonstrates that incorporated Ag particles can boost electron transfer and Li$^+$ transfer, which significantly influence electrochemical performance.

4   Conclusions

As an anode material, $Li_4Ti_5O_{12}$ is a promising candidate for use in lithium rechargeable batteries in order to solve the safety issues, although the low kinetics associated with its poor electrical conductivity

limits the electrochemical performance from the viewpoint of practical application. We have demonstrated an effective way to improve the kinetics of $Li_4Ti_5O_{12}$ toward fast Li^+ intercalation/de-intercalation by incorporation of Ag nanoparticles. The Ag–$Li_4Ti_5O_{12}$ nanofibers exhibit high specific capacity, and remarkably high rate capability and cycling performance due to higher conductivity and faster Li^+ diffusion compared with pristine $Li_4Ti_5O_{12}$. The controlled incorporation of Ag nanoparticles into 1D $Li_4Ti_5O_{12}$ nanostructures is a promising approach to improve electrochemical performance in advanced Li^+ storage devices.

Acknowledgements

References

[1] Jeong, G.; Kim, Y. U.; Kim, H.; Kim, Y. J.; Sohn, H. J. Prospective materials and applications for Li secondary batteries. *Energy Environ. Sci.* **2011**, *4*, 1986–2002.

[2] Deng, D.; Kim, M. G.; Lee, J. Y.; Cho, J. Green energy storage materials: Nanostructured TiO_2 and Sn-based anodes for lithium-ion batteries. *Energy Environ. Sci.* **2009**, *2*, 818–837.

[3] Colbow, K. M.; Dahn J. R.; Haering, R. R. Structure and electrochemistry of the spinel oxides $LiTi_2O_4$ and $Li_{4/3}Ti_{5/3}O_4$. *J. Power Sources* **1989**, *26*, 397–402.

[4] Ferg, E.; Gummow, R. J.; de Kock, A.; Thackeray, M. M. Spinel anodes for lithium-ion batteries. *J. Electrochem. Soc.* **1994**, *141*, L147–L150.

[5] Ohzuku, T.; Ueda, A.; Yamamoto, N. Zero-strain insertion material of $Li[Li_{1/3}Ti_{5/3}]O_4$ for rechargeable lithium cells. *J. Electrochem. Soc.* **1995**, *142*, 1431–1435.

[6] Kavan, L.; Gratzel, M. Facile synthesis of nanocrystalline $Li_4Ti_5O_{12}$(spinel) exhibiting fast Li insertion. *Electrochem. Solid-State Lett.* **2002**, *5*, A39–A42.

[7] Lu, X.; Zhao, L.; He, X.; Xiao, R.; Gu, L.; Hu, Y.-S.; Li, H.; Wang, Z.; Duan, X.; Chen, L.; et al. Lithium storage in $Li_4Ti_5O_{12}$ spinel: The full static picture from electron microscopy. *Adv. Mater.* **2012**, *24*, 3233–3268.

[8] Pan, H.; Zhao, L.; Hu, Y.-S.; Li, H.; Chen, L. Improved Li-storage performance of $Li_4Ti_5O_{12}$ coated with C–N compounds derived from pyrolysis of urea through a low-temperature approach. *ChemSusChem* **2012**, *5*, 526–529.

[9] Pan, H.-L.; Hu, Y.-S.; Li, H.; Chen, L.-Q. Significant effect of electron transfer between current collector and active material on high rate performance of $Li_4Ti_5O_{12}$. *Chin. Phys. B* **2011**, *20*, 118202.

[10] Jansen, A. N.; Kahaian, A. J.; Kepler, K. D.; Nelson, P. A.; Amine, K.; Dees, D. W.; Vissers, D. R.; Thackeray, M. M. Development of a high-power lithium-ion battery. *J. Power Sources* **1999**, *81–82*, 902–905.

[11] Ouyang, C. Y.; Zhong, Z. Y.; Lei, M. S. *Ab initio* studies of structural and electronic properties of $Li_4Ti_5O_{12}$ spinel. *Electrochem. Commun.* **2007**, *9*, 1107–1112.

[12] Wang, Y.-Q.; Gu, L.; Guo, Y.-G.; Li, H.; He, X.-Q.; Tsukimoto, S.; Ikuhara, Y.; Wan, L.-J. Rutile–TiO_2 nanocoating for a high-rate $Li_4Ti_5O_{12}$ anode of a lithium-ion battery. *J. Am. Chem. Soc.* **2012**, *134*, 7874–7879.

[13] Han, H.; Song, T.; Bae, J. Y.; Nazar, L. F.; Kim, H.; Paik, U. Nitridated TiO_2 hollow nanofibers as an anode material for high power lithium ion batteries. *Energy Environ. Sci.* **2011**, *4*, 4532–4536.

[14] Park, K. S.; Benayad, A.; Kang, D. J.; Doo, S. G. Nitridation-driven conductive $Li_4Ti_5O_{12}$ for lithium ion batteries. *J. Am. Chem. Soc.* **2008**, *130*, 14930–14931.

[15] Seo, M. H.; Park, M.; Lee, K. T.; Kim, K.; Kim, J.; Cho, J. High performance Ge nanowire anode sheathed with carbon for lithium rechargeable batteries. *Energy Environ. Sci.* **2011**, *4*, 425–428.

[16] Nugroho, A.; Chang, W.; Kim, S. J.; Chung, K. Y.; Kim, J. Superior high rate performance of core–shell $Li_4Ti_5O_{12}$/carbon nanocomposite synthesized by a supercritical alcohol approach. *RSC Adv.* **2012**, *2*, 10805–10808.

[17] Lee, S.; Cho, Y.; Song, H.-K.; Lee, K. T.; Cho, J. Carbon-coated single-crystal $LiMn_2O_4$ nanoparticle clusters as cathode material for high-energy and high-power lithium-ion batteries. *Angew. Chem. Int. Edit.* **2012**, *51*, 8748–8752.

[18] Cai, R.; Jiang, S. M.; Yu, X.; Zhao, B. T.; Wang, H. T.; Shao, Z. P. A novel method to enhance rate performance of an Al-doped $Li_4Ti_5O_{12}$ electrode by post-synthesis treatment in liquid formaldehyde at room temperature. *J. Mater. Chem.* **2012**, *22*, 8013–8021.

[19] Song, H.; Yun, S.-W.; Chun, H.-H.; Kim, M.-G.; Chung, K. Y.; Kim, H. S.; Cho, B.-W.; Kim, Y.-T. Anomalous decrease in structural disorder due to charge redistribution in Cr-doped $Li_4Ti_5O_{12}$ negative-electrode materials for high-rate Li-ion batteries. *Energy Environ. Sci.* **2012**, *5*, 9903–9913.

[20] Gu, F.; Chen, G.; Wang, Z. Synthesis and electrochemical performances of $Li_4Ti_{4.95}Zr_{0.05}O_{12}$/C as anode material for lithium-ion batteries. *J. Solid State Electrochem.* **2012**, *16*, 375–382.

[21] Nam, S. H.; Shim, H. S.; Kim, Y. S.; Dar, M. A.; Kim, J. G.; Kim, W. B. Ag or Au nanoparticle-embedded one-dimensional composite TiO_2 nanofibers prepared via electrospinning for

use in lithium-ion batteries. *ACS Appl. Mater. Inter.* **2010**, *2*, 2046–2052.

[22] Du, G.; Sharma, N.; Peterson, V. K.; Kimpton, J. A.; Jia, D.; Guo, Z. Br-doped $Li_4Ti_5O_{12}$ and composite TiO_2 anodes for Li-ion batteries: Synchrotron X-ray and *in situ* neutron diffraction studies. *Adv. Funct. Mater.* **2011**, *21*, 3990–3997.

[23] Guo, Y.-G.; Hu, Y.-S.; Sigle, W.; Maier, J. Superior electrode performance of nanostructured mesoporous TiO_2 (anatase) through efficient hierarchical mixed conducting networks. *Adv. Mater.* **2007**, *19*, 2087–2091.

[24] Kim, J.-G.; Shi, D.; Kong, K.-J.; Heo, Y.-U.; Kim, J. H.; Jo, M. R.; Lee, Y. C.; Kang, Y.-M.; Dou, S. X. Structurally and electronically designed TiO_2N_x nanofibers for lithium rechargeable batteries. *ACS Appl. Mater. Interfaces* **2013**, *5*, 691–696.

[25] Shim, H. W.; Lee, D. K.; Cho, I. S.; Hong, K. S.; Kim, D. W. Facile hydrothermal synthesis of porous TiO_2 nanowire electrodes with high-rate capability for Li ion batteries. *Nanotechnology* **2010**, *21*, 255706.

[26] Xia, Y.; Yang, P.; Sun, Y.; Wu, Y.; Mayers, B.; Gates, B.; Yin, Y.; Kim, F.; Yan, H. One-dimentional Nanostructures: Synthesis, Characterization, and Applications. *Adv. Mater.* **2003**, *15*, 353–389.

[27] Lu, X.; Wang, C.; Wei, Y. One-dimensional composite nano-materials: Synthesis by electrospinning and their applications. *Small* **2009**, *5*, 2349–2370.

[28] Jo, M. R.; Jung, Y. S.; Kang, Y.-M. Tailored $Li_4Ti_5O_{12}$ nanofibers with outstanding kinetics for lithium rechargeable batteries. *Nanoscale*, **2012**, *4*, 6870–6875

[29] Li, D.; Xia, Y. Fabrication of titania nanofibers by electro-spinning. *Nano Lett.* **2003**, *3*, 555–560.

[30] Li, D.; Xia, Y. Direct fabrication of composite and ceramic hollow nanofibers by electrospinning. *Nano Lett.* **2004**, *4*, 933–938.

[31] Yu, Y.; Gu, L.; Zhu, C.; Aken, P. A.; Maier, J. Tin nano-particles encapsulated in porous multichannel carbon microtubes: Preparation by single-nozzle electrospinning and application as anode material for high-performance Li-based batteries. *J. Am. Chem. Soc.* **2009**, *131*, 15984–15985.

[32] Cavaliere, S.; Subianto, S.; Savych, I.; Jones, D. J.; Roziere, J. Electrospinning: Designed architectures for energy

conversion and storage devices. *Energy Environ. Sci.* **2011**, *4*, 4761–4785.

[33] Asokan, K.; Park, J. Y.; Choi, S.; Chang, C.; Kim, S. S. Stabilization of the anatase phase of $Ti_{1-x}Sn_xO_2$ ($x < 0.5$) nanofibers. *Nano Res.* **2010**, *3*, 256–263.

[34] Kim, J.; Cho, J. Spinel $Li_4Ti_5O_{12}$ nanowires for high-rate Li-ion intercalation electrode. *Electrochen Solid-State Lett.* **2007**, *10*, A81–A84.

[35] Aldon, L.; Kubiak, P.; Womes, M.; Jumas, J. C.; Olivier-Fourcade, J.; Tirado, J. L.; Corredor, J. I.; Vicente, C. P. Chemical and electrochemical Li-insertion into the $Li_4Ti_5O_{12}$ spinel. *Chem. Mater.* **2004**, *16*, 5721–5725.

[36] Wan, Z.; Cai, R.; Jiang, S.; Shao, Z. Nitrogen- and TiN-modified $Li_4Ti_5O_{12}$: One-step synthesis and electrochemical performance optimization. *J. Mater. Chem.* **2012**, *22*, 17773–17781.

[37] Huang, S.; Wen, Z.; Zhu, X.; Gu, Z. Preparation and electro-chemical performance of Ag doped $Li_4Ti_5O_{12}$. *Electrochem. Commun.* **2004**, *6*, 1093–1097.

[38] Liu, Z.; Zhang, N.; Wang, Z.; Sun, K. Highly dispersed Ag nanoparticles (<10 nm) deposited on nanocrystalline $Li_4Ti_5O_{12}$ demonstrating high-rate charge/discharge capability for lithium-ion battery. *J. Power Sources* **2012**, *205*, 479–482.

[39] Herle, P. S.; Ellis, B.; Coombs, N.; Nazar, L. F. Nano-network electronic conduction in iron and nickel olivine phosphates. *Nat. Mater.* **2004**, *3*, 147–152.

[40] Suo, L.; Hu, Y.-S.; Li, H.; Armand, M.; Chen, L. A new class of solvent-in-salt electrolyte for high-energy rechargeable metallic lithium batteries. *Nat. Commun.* **2013**, *4*, 1481.

[41] Jo, M. R.; Nam, K. M.; Lee, Y.; Song, K.; Park, J. T.; Kang, Y.-M. Phosphidation of $Li_4Ti_5O_{12}$ nanoparticles and their electrochemical and biocompatible superiority for lithium rechargeable batteries. *Chem. Commun.* **2011**, *47*, 11474–11476.

[42] Zhao, L.; Hu, Y. S.; Li, H.; Wang, Z. X.; Chen, L. Q. Porous $Li_4Ti_5O_{12}$ coated with N-doped carbon from ionic liquids for Li-ion batteries. *Adv. Mater.* **2011**, *23*, 1385–1388.

[43] Ma, Y.; Ji, G.; Ding, B.; Lee, J. Y. Facile solvothermal synthesis of anatase TiO_2 microspheres with adjustable mesoporosity for the reversible storage of lithium ions. *J. Mater. Chem.* **2012**, *22*, 24380–24385.